ndt

MDPI

*Article*

# An Experimental Study of Machine-Learning-Driven Temperature Monitoring for Printed Circuit Boards (PCBs) Using Ultrasonic Guided Waves

**Lawrence Yule [1,*], Nicholas Harris [1], Martyn Hill [2] and Bahareh Zaghari [3]**

[1] Smart Electronic Materials and Systems Research Group, School of Electronics and Computer Science, University of Southampton, Southampton SO17 1BJ, UK; nrh@ecs.soton.ac.uk
[2] Mechatronics Research Group, School of Engineering, University of Southampton, Southampton SO17 1BJ, UK; m.hill@soton.ac.uk
[3] Electrical Power Engineering (EPE) Research Group, School of Electronics and Computer Science, University of Southampton, Southampton SO17 1BJ, UK; bahareh.zaghari@soton.ac.uk
* Correspondence: yulelawrence@gmail.com

**Abstract:** Temperature has a significant impact on the operational lifetime of electronic components, as excessive heat can lead to accelerated degradation and ultimately failure. In safety-critical applications, it is important that real-time monitoring is employed to reduce the risk of system failures and maintain the safety, reliability, and integrity of the connected systems. In the case of printed circuit boards (PCBs), it is often not feasible to install enough sensors to adequately cover all of the temperature sensitive components. In this study, we present a novel method for the temperature monitoring of PCBs using ultrasonic guided waves and machine learning techniques. Our approach utilizes a small number of low-cost, unobtrusive piezoelectric wafer active sensors (PWAS) sensors for propagating ultrasonic guided waves across a PCB. Through interaction with board features, the temperature of components can be predicted using multi-output regression algorithms. Our technique has been applied to three different PCBs, each with five hotspot positions, achieving an RMSE of <3.5 °C and $R^2 > 0.95$ in all three cases.

**Keywords:** condition monitoring; ultrasonic guided waves; printed circuit boards; PWAS; temperature monitoring



Academic Editor: Fabio Tosti

Received: 29 August 2024
Revised: 2 December 2024
Accepted: 16 December 2024
Published: 1 January 2025

**Citation:** Yule, L.; Harris, N.; Hill, M.; Zaghari, B. An Experimental Study of Machine-Learning-Driven Temperature Monitoring for Printed Circuit Boards (PCBs) Using Ultrasonic Guided Waves. *NDT* **2025**, *3*, 1. https://doi.org/10.3390/ndt3010001



## 1. Introduction

In safety-critical applications, such as those found in the aerospace and automotive industries, the real-time temperature monitoring of Printed Circuit Boards (PCBs) is an important area that is yet to be fully considered. By implementing real-time temperature monitoring, these industries could benefit from a predictive maintenance strategy, which focuses on addressing problems before they result in system failures. Unlike traditional reactive maintenance, where components are replaced after failure, or preventative maintenance, which relies on scheduled servicing, predictive maintenance uses real-time data to forecast when a component is likely to fail. This approach not only reduces downtime and repair costs but also extends the operational life of the system. In aerospace, PCBs are embedded in flight control systems, avionics, and navigation equipment that are subjected to wide temperature ranges and harsh operating conditions. Real-time temperature monitoring could provide early warning of temperature-induced stress or imminent component failure, and allow for the dynamic adjustment of cooling mechanisms or switching to redundant systems, enhancing both reliability and safety. This also extends to the automotive

industry, where modern vehicles are increasingly dependent on electronics for critical functions such as engine control, braking systems, and autonomous driving capabilities. As these electronic systems evolve to include more sophisticated technologies like advanced driver-assistance systems (ADAS), temperature management becomes even more important. Potential failures can be prevented by identifying and addressing overheating, as temperature fluctuations often precede component degradation or failure. By detecting these warning signs in real time, proactive measures can be taken through the use of active control systems, pre-emptive maintenance, or the replacement of components. This contributes to improvements in reliability and the mitigation of safety risks.

During the manufacturing process, various techniques are employed to detect defects before PCBs are approved for mass production. Traditionally, this inspection could be performed manually by a trained technician. However, as solder joints become smaller and the number of potential defects increases, manual inspection is becoming less feasible. Instead, automated optical inspection (AOI) is increasingly used. AOI leverages image processing techniques to identify defects by comparing the inspected board to a reference image [1]. Machine learning methods are also being integrated to enhance detection accuracy and speed [2,3]. Despite their effectiveness in controlled manufacturing environments, these methods are not suitable for real-time, in-operation monitoring of PCBs. Temperature, a common source of defects, is not directly addressed during this stage. To monitor temperature, several techniques can be employed, including thermocouples, thermal cameras, and onboard chip temperature sensors.

Thermocouples can be used to temporarily monitor temperature at specific points and assess soldering quality during the hot air reflow soldering process [4]. However, it is often impractical to apply a sensor to every component of interest, especially as component density increases [5]. Infrared (IR) cameras can visualize temperature distributions across the PCB surface [6,7]. While IR cameras offer a non-contact and comprehensive view of temperature profiles, they are expensive and not feasible for real-time monitoring due to space and power constraints. They also require the board to be coated with a material that provides consistent emissivity, as metal elements (solder, leads, connectors, etc.) are highly reflective to infrared light. Onboard chip temperature sensors are effective at monitoring the temperature of specific ICs [8], but are not commonly found in simple resistor or capacitor packages. Digital temperature sensors can be daisy-chained to provide a distributed monitoring system across a board [9], but this requires additional components, which may not be feasible if components are densely packed, and requires appropriate monitoring to be considered during the design stage.

Alternative approaches include inferring onboard temperatures from offboard measurements by linking temperature measurements near the PCB board to onboard temperatures using neural networks [10], distributed temperature monitoring using optical fibre sensors [11], measuring changes in dielectric constant via resonant frequency [12], and 'life consumption' analysis, which measures the effect of temperature and vibration on PCB solder joints and calculates the remaining life of the system [13].

In this study, we propose a novel method for the temperature monitoring of PCBs using ultrasonic guided waves (UGW). The use of UGWs is well established in non-destructive evaluation and structural health monitoring [14], where they are used to inspect a variety of structures for defects and damage, such as wind turbines [15], pipelines [16], aircraft [17], and rails [18]. However, there are only a limited number of studies that consider ultrasonic waves for temperature monitoring applications, as in most cases traditional temperature monitoring approaches are more applicable. Jia and Skliar [19] developed a system of measuring temperature distribution across the wall of a oxy-fuel combustor by tracking changes in time of flight from reflections at points along a waveguide. A similar system

using a combination of longitudinal and shear waves to measure both thickness and temperature is described by Zhang and Cegla [20]. Surface acoustic wave (SAW) devices can be utilized for wireless temperature measurement, by measuring a change in resonant frequency with temperature [21]. There are only a limited number of papers that specifically consider the use of UGWs for temperature sensing [22,23].

Despite this, we consider UGWs to be highly suitable for real-time temperature monitoring of PCBs. A small number of low-cost, unobtrusive, piezoelectric wafer active sensors (PWAS) can be used to propagate guided waves across a PCB. By analyzing the complex signals generated through interactions with board features, the temperature of components can be accurately predicted using multi-output regression algorithms. These algorithms are capable of identifying the subtle temperature effects embedded within the signals that occur at different hotspot positions across a board.

## 2. Methodology

Building on our previous work [24], we propose a novel methodology for monitoring the thermal state of a Printed Circuit Board (PCB). Sensors are strategically placed on the PCB, away from sensitive components, to ensure non-intrusive measurement while still capturing the necessary thermal signatures. The key idea is to transmit guided ultrasonic wave pulses from an actuator and record their propagation at multiple receiver locations. As these waves travel across the PCB, they interact with various features including geometries, material boundaries, and thermal gradients. This interaction leads to wave scattering and reflection, resulting in a complex signal that contains valuable embedded information about temperature changes.

A temperature hotspot originating from a component will propagate heat onto the PCB surface through their pins/legs, which are connected to a board through solder joints and pads. This results in a temperature gradient extending out from the component position, which ultrasonic guided waves are affected by as they propagate. These waves are constrained between the upper and lower boundaries of the board, and so any temperature change, both on the surface and through the cross-section, is monitored by this method.

Traditional signal processing techniques, such as linking temperature change to time-of-flight (ToF) or amplitude, are insufficient for capturing the full extent of the thermal information embedded within these complex signals. To overcome these challenges, we propose the use of machine learning (ML) algorithms to predict the temperature at multiple known hotspot locations on the PCB simultaneously. The advantage of an ML approach lies in the ability to extract intricate patterns and relationships from high-dimensional data. By training ML models on labeled data that include waveforms and corresponding temperature readings from known hotspots, the models can learn to associate specific signal characteristics with thermal states across different regions of the PCB.

After training and evaluating multiple machine learning models, the results are compared based on their Root Mean Squared Error (RMSE) and $R^2$ scores. Models that achieve lower RMSE and higher $R^2$ values are ranked higher. Through this process, we identify the best-performing algorithms for temperature prediction at different hotspot positions on the PCB. Python's sci-kit learn package [25] is used for feature scaling, model training, hyperparameter tuning, and evaluation.

### 2.1. Sensors

PWAS are cheap, small, and ideally suited to the excitation of guided waves. The in-plane motion of the sensor is coupled with the particle motion of Lamb waves on the material surface when driven by an external voltage [26]. We are using PWAS measuring 6.50 × 0.27 mm with wrap-around electrode patterns (APC International Ltd. (Mackeyville,

PA, USA) 851/Navy Type II/PZT-5A: $d_{33}$ 400 $\times$ $10^{-12}$ m/V, $d_{31}$ $-210$ $\times$ $10^{-12}$ m/V, $Q_m$ 80), which are small enough to be mounted in multiple locations without affecting the operation of a board.

Operating frequency is dictated by sensor diameter, as although PWAS are not resonant devices, they still have an optimal working frequency range, which is centered around odd multiples of $\lambda/2$ for the mode of interest. In this case, a diameter of 6.5 mm translates to an optimal frequency of $\sim$300 kHz when targeting the use of the lowest-order symmetric mode, $S_0$. The $S_0$ mode is more appropriate than $A_0$ (lowest-order asymmetric mode) for this application, as greater amplitudes can be achieved with the same excitation voltage. The operational sweet spot occurs at a higher frequency, where more reflection/scattering can be expected from small components as the wavelength of the signal is more comparable with their size. In many uses of ultrasonic guided waves for condition monitoring, single-mode operation is preferable as it simplifies signal processing and analysis. When machine learning is employed, however, this may not be the case, as it may be advantageous to work with a more complex signal, containing more features that can be extracted and linked to a change in a target variable. We have not attempted to eliminate the presence of the $A_0$ mode in our signal for this reason.

### *2.2. Test PCBs*

Three PCBs have been used to test the proposed temperature monitoring technique. Two boards have been designed with temperature controllable hotspots, where PCB #1 has evenly spaced components (Figure 1a) and PCB #2 has them arranged in a closely aligned array (Figure 2a). PCB #3 (Figure 3a) has heat applied externally to unpowered ICs, to demonstrate the principal of training ML models on a production board. In all three cases, the boards have five hotspot positions present.

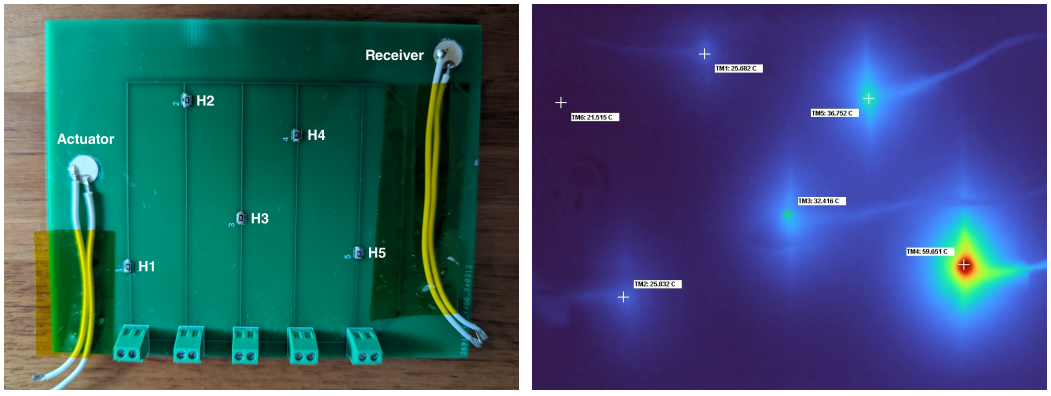


(**a**) (**b**)

**Figure 1.** (**a**) Test PCB #1. Resistor hotspots are denoted H1–5. (**b**) IR camera image of PCB #1.

Both PCB #1 and #2 have the same dimensions, 99.0 $\times$ 77.5 $\times$ 1.6 mm. The resistors used as hotspots are all 0805 type (2012 metric), 200 $\Omega$, 0.5 W. PCB #2 has an additional receiver PWAS present. On PCB #3 (see Figure 3a), heat is applied to the onboard ICs via external 2512-type (6432 metric) resistors. A thin layer of 'superglue' (Ethyl 2-cyanoacrylate) is used to bond the external resistor to the onboard IC housing. As seen in Figure 3b, heat is being transferred from the external resistors into the IC housing, and through the pins, into the PCB. This replicates the heating of the components through onboard operation, as seen on PCB #1 and #2. Two receiver PWAS are used. In all cases the voltage across each resistor is incremented by 0.5 V, which corresponds to $\sim$5 °C, from 3.5 to 9.0 V, or 30–90 °C. The temperature of each hotspot is allowed to stabilize for 3 mins before signals are captured.

Each hotspot position is ramped up in temperature over the full range, and then allowed to return to room temperature, before moving to the next hotspot position.

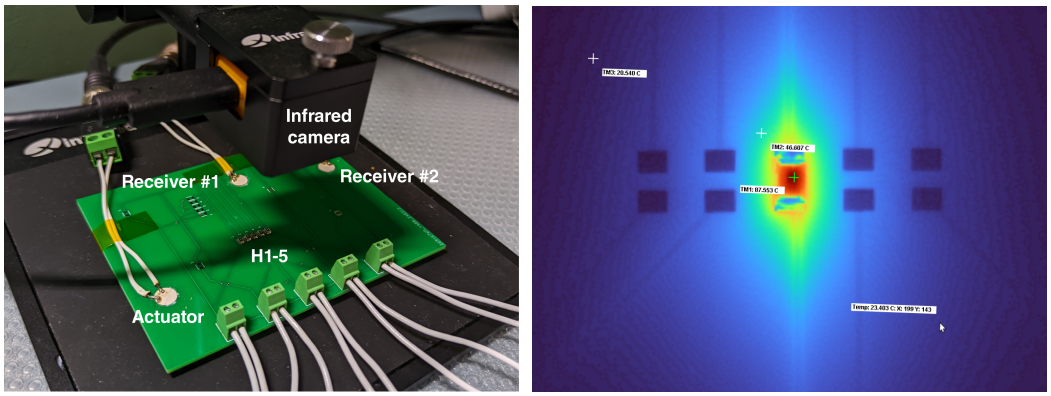


(**a**) (**b**)

**Figure 2.** (**a**) Test PCB #2. Resistor hotspots are denoted H1–5. (**b**) IR camera image of PCB #2.

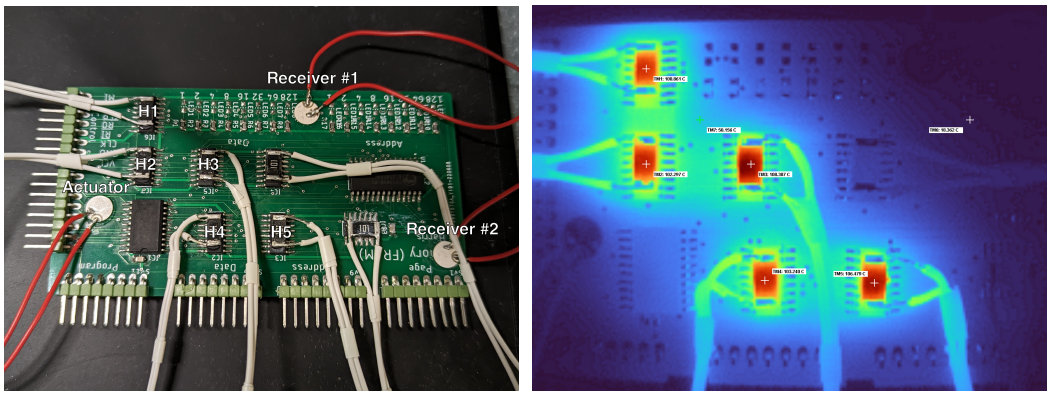


(**a**) (**b**)

**Figure 3.** (**a**) Test PCB #3 with externally applied hotspots (H1–5). (**b**) IR camera image of PCB #3.

### *2.3. Test Procedure*

An arbitrary waveform generator (GW Instek MFG-2230M) is used to generate a 300 kHz, five-cycle Hann windowed pulse, internally triggered at a rate of 100 ms. A Picoscope 3406D MSO USB oscilloscope is used to digitize the signals, at a sampling rate of 5 MHz. Signals are captured on a trigger from the excitation pulse, 200 µs with a 5% pre-trigger. A high-pass filter is used to remove any DC offset. The temperature of the components and the boards themselves are monitored using an infrared camera (Xinfrared T2S Plus), in combination with 'IRCAM Thermal Viewer' software (RMG-Engineering, v2.1.5). Measurement points are placed at the center of each hotspot position, as seen in Figures 1–3, and sampled at a rate of 20 Hz. The camera is positioned directly above the board, as seen in Figure 2, ensuring that the image is focused, and each hotspot position is clearly visible. The temperature measurements are associated with each ultrasonic signal by the closest timestamp.

A large number of features are calculated from each signal, which can be split into three sections, overall features, binned features, and peak amplitudes. The overall features are made up of the mean, standard deviation, skewness, kurtosis, median, min, max, range, sum, and variance. These features are then calculated for different parts of the signal, after splitting into ten equally spaced bins. Finally, the envelope of the original signal is calculated, and the amplitude of the five most prominent peaks are measured. An example of how the signals are processed is shown in Figure 4 for PCB#1.

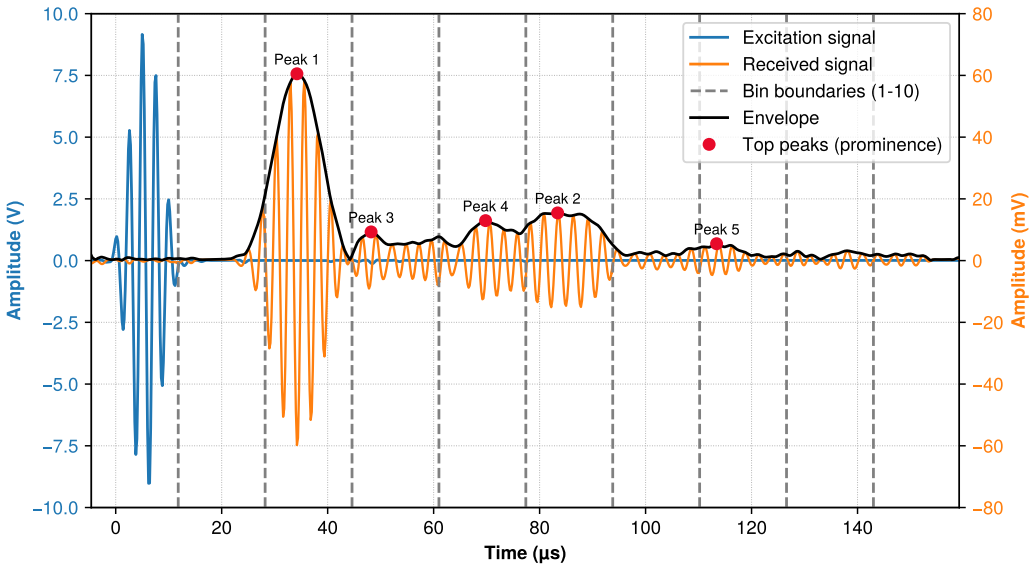


**Figure 4.** Example of signal waveforms on PCB #1 at 25 °C.

Features are scaled using sklearn 'StandardScaler', which normalizes their distributions. As there are many features (93), it is advisable to reduce dimensionality by removing those least correlated with the target variable (temperature), reducing training time and potentially improving model performance. Firstly, a correlation matrix is generated to determine if any two features are perfectly correlated, in which case one is removed from the dataset. The reduced subset of features is then ranked based on mutual information regression score for the first hotspot position of each board, as shown in Table 1. Figures 5–7 show the correlation matrices post-removal of highly correlated features (a) and the change in RMSE when a range of models are trained with an increasing number of features (b).

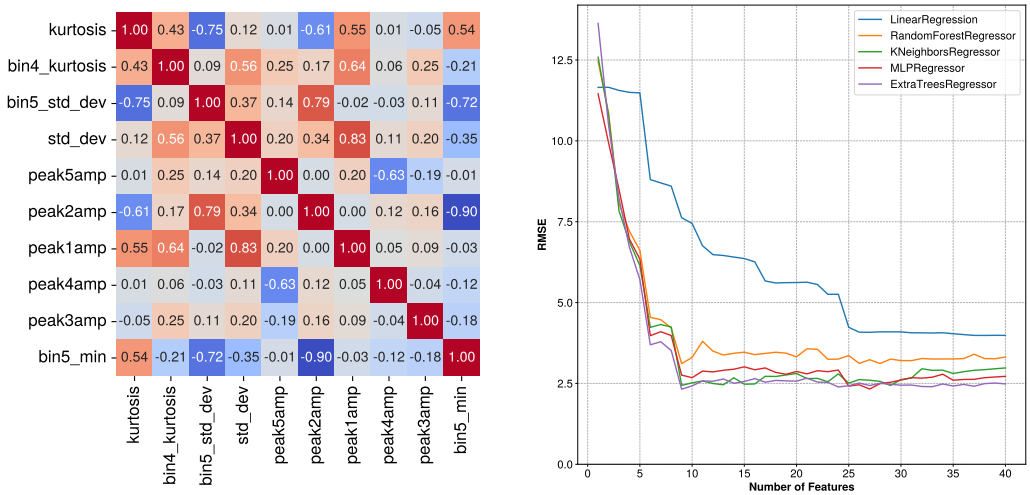


(**a**) (**b**)

**Figure 5.** Feature selection for PCB #1. (**a**) Ranked correlation matrix of the top 10 features. Red indicates positive correlation, blue indicates negative correlation. (**b**) Change in RMSE when models are trained with an increasing number of top features, as determined by the mutual information regression score.

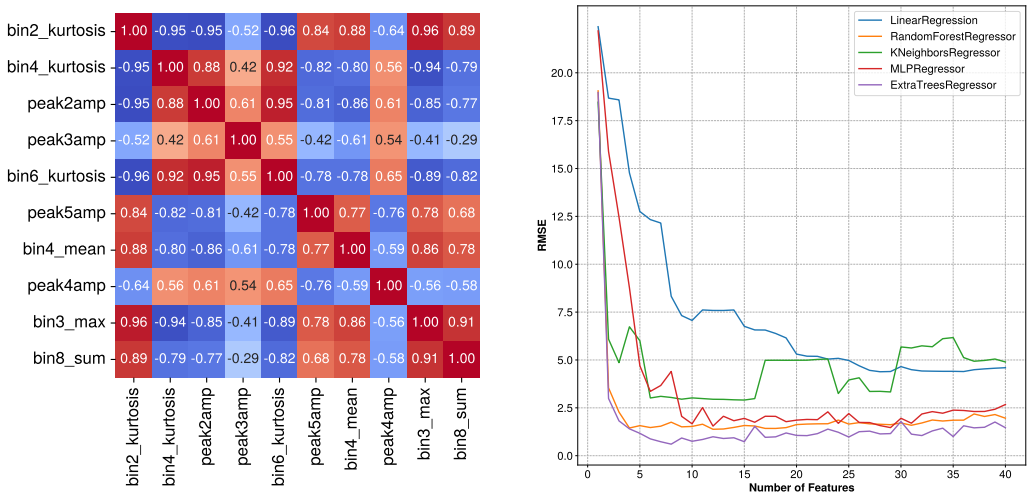


(**a**) (**b**)

**Figure 6.** Feature selection for PCB #2. (**a**) Ranked correlation matrix of the top 10 features. Red indicates positive correlation, blue indicates negative correlation. (**b**) Change in RMSE when models are trained with an increasing number of top features, as determined by the mutual information regression score.

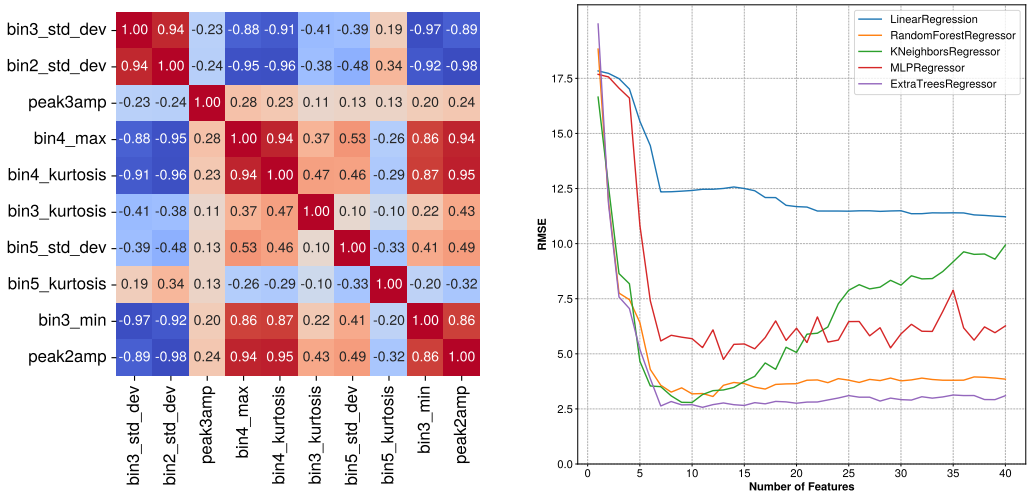


(**a**) (**b**)

**Figure 7.** Feature selection for PCB #3. (**a**) Ranked correlation matrix of the top 10 features. Red indicates positive correlation, blue indicates negative correlation. (**b**) Change in RMSE when models are trained with an increasing number of top features, as determined by the mutual information regression score.

In general, the most important features are those calculated on the bins corresponding to reflection/scattering of the direct signal, which can be seen by comparing the feature bins in Table 1 with Figure 4. The most important features do vary significantly between boards, however, as the influence of temperature on the reflected/scattered signal differs depending on sensor placement and the layout of components. The improvement in RMSE for all models begins to stabilize at ∼10 features. In some cases (particularly 'KNeighborsRegressor'), the addition of features with limited correlation to the target variable causes RMSE to increase above this number of features. Based on this result across the three boards, the top 20 features are selected and passed on to model training. K-fold cross validation (n_splits = 5) is used in all cases. This provides a more robust estimate of model performance compared to a single train-test split, helping to reduce overfitting.

**Table 1.** Most important features as ranked by the mutual information score for regression.

| Feature | Score |
|---|---|
| (a) PCB #1 | |
| kurtosis | 0.57 |
| bin4_kurtosis | 0.48 |
| bin5_std_dev | 0.47 |
| std_dev | 0.46 |
| peak5amp | 0.45 |
| peak2amp | 0.37 |
| peak1amp | 0.34 |
| peak4amp | 0.33 |
| peak3amp | 0.28 |
| bin5_min | 0.25 |
| (b) PCB #2 | |
| bin2_kurtosis | 2.21 |
| bin4_kurtosis | 1.90 |
| peak2amp | 1.71 |
| peak3amp | 1.67 |
| bin6_kurtosis | 1.38 |
| peak5amp | 1.35 |
| bin4_sum | 1.34 |
| peak4amp | 1.21 |
| bin3_max | 1.06 |
| bin8_sum | 0.90 |
| (c) PCB #3 | |
| bin3_std_dev | 0.63 |
| bin2_std_dev | 0.60 |
| bin4_max | 0.50 |
| peak3amp | 0.50 |
| bin4_kurtosis | 0.49 |
| bin3_kurtosis | 0.41 |
| bin5_std_dev | 0.36 |
| bin5_kurtosis | 0.33 |
| bin3_min | 0.32 |
| peak2amp | 0.32 |

For PCB #1, using an 80/20 split of train/test data results in 2156 samples of train data and 540 samples of test data. For PCB #2, using an 80/20 split of train/test data results in 265 samples of train data and 67 samples of test data. A limited number of samples are used in this test, to evaluate the ability of the models against the use of significantly more training data for PCB #1/3. For PCB #3, using an 80/20 split of train/test data results in 1601 samples of train data and 401 samples of test data.

A range of regression models are trained on the feature subset, and their prediction accuracies compared based on RMSE and $R^2$. The default hyperparameters as provided by sklearn are used during this stage, and only the 'max_iter' parameter is increased to ensure that certain models are fit. After the most effective model has been determined, their hyperparameters are tuned using 'RandomizedSearchCV' to further improve their performance. The finalized model is then used to predict unseen test data.

## 3. Results and Discussion

Figures 8–10 show the result of training multiple regression models to predict the temperature of five hotspots simultaneously, across the three test PCBs. The RMSE and $R^2$ values are reported as a mean average of the five hotspot scores, along with the standard deviation.

In all three cases, the most effective regression model was 'ExtraTreesRegressor', achieving an average RMSE of <3.5 °C, and an $R^2$ of ≥0.95. The result of the tests on PCBs #1 and 2 shows that the position of the sensors, and the arrangement of the components, does not significantly affect the accuracy of the ML predictions.

The result from PCB #2 highlights the ability of the system to effectively distinguish between hotspot positions, even when they are closely aligned/spaced. The reduced size of the dataset is also of note, as the test set contains data points at temperatures unseen to in the training data, which suggests that the method is not reliant on a comprehensive training data set. Having said that, the greater variability in the result, both in terms of overall model performance, and the RMSE across the five components for the same model, suggests that a larger training set would be beneficial.

| Model | RMSE | $R^2$ |
|---|---|---|
| ExtraTreesRegressor | 2.47 ± 0.08 | 0.97 |
| MLPRegressor | 2.55 ± 0.09 | 0.96 |
| RandomForestRegressor | 2.92 ± 0.18 | 0.95 |
| KNeighborsRegressor | 3.01 ± 0.14 | 0.95 |
| HistGradientBoostingRegressor | 3.03 ± 0.24 | 0.95 |
| GradientBoostingRegressor | 3.09 ± 0.14 | 0.94 |
| DecisionTreeRegressor | 4.37 ± 0.53 | 0.89 |
| LinearRegression | 6.06 ± 0.13 | 0.80 |
| LassoCV | 6.06 ± 0.22 | 0.80 |
| BayesianRidge | 6.06 ± 0.10 | 0.80 |

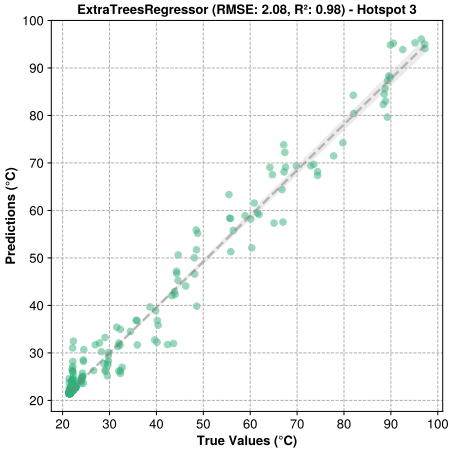


**Figure 8.** Results for PCB #1, showing (**left**) regression models ranked by RMSE, with the average RMSE and R² across five hotspot predictions, and (**right**) regression result using 'ExtraTreesRegressor' for hotspot position 3.

| Model | RMSE | $R^2$ |
|---|---|---|
| ExtraTreesRegressor | 1.72 ± 0.51 | 0.99 |
| GradientBoostingRegressor | 3.29 ±0.32 | 0.95 |
| RandomForestRegressor | 4.36 ± 0.85 | 0.9 |
| HistGradientBoostingRegressor | 4.89 ± 0.43 | 0.92 |
| DecisionTreeRegressor | 5.13 ± 1.67 | 0.88 |
| KNeighborsRegressor | 7.12 ± 0.76 | 0.76 |
| LinearRegression | 7.96 ± 0.61 | 0.77 |
| LassoCV | 8.37 ± 0.75 | 0.72 |
| BayesianRidge | 8.50 ± 0.45 | 0.72 |
| MLPRegressor | 11.17 ± 0.78 | 0.56 |

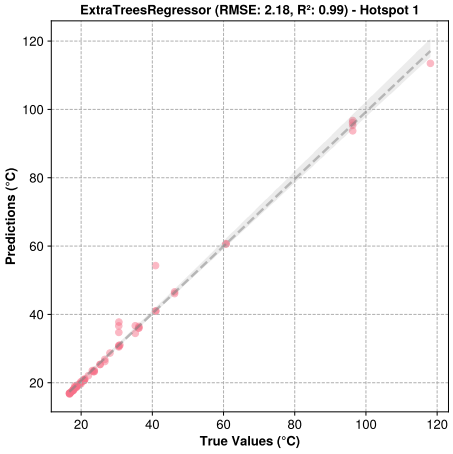


**Figure 9.** Results for PCB #2, showing (**left**) regression models ranked by RMSE, with the average RMSE and R² across five hotspot predictions, and (**right**) regression result using 'ExtraTreesRegressor' for hotspot position 1.

| Model | RMSE | $R^2$ |
|---|---|---|
| ExtraTreesRegressor | $3.41 \pm 0.15$ | 0.95 |
| KNeighborsRegressor | $4.29 \pm 0.50$ | 0.92 |
| HistGradientBoostingRegressor | $4.60 \pm 0.32$ | 0.92 |
| MLPRegressor | $4.74 \pm 0.23$ | 0.89 |
| RandomForestRegressor | $4.75 \pm 0.23$ | 0.92 |
| GradientBoostingRegressor | $4.84 \pm 0.25$ | 0.90 |
| DecisionTreeRegressor | $6.44 \pm 0.64$ | 0.81 |
| AdaBoostRegressor | $7.08 \pm 0.32$ | 0.81 |
| BayesianRidge | $11.63 \pm 0.20$ | 0.50 |
| ARDRegression | $11.64 \pm 0.22$ | 0.51 |

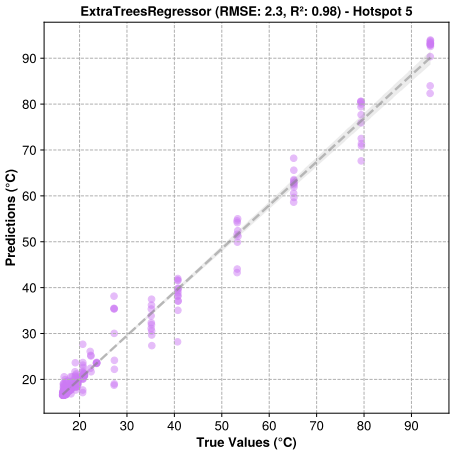


**Figure 10.** Results for PCB #3, showing (**left**) regression models ranked by RMSE, with average RMSE and $R^2$ across five hotspot predictions, and (**right**) regression result using 'ExtraTreesRegressor' for hotspot position 5.

The result for PCB #3 is particularly interesting, as it suggests that applying heat externally is a valid method of training ML models for this task, which would it to be applied to any PCB. These results are based on the use of two receivers; however, if 'ExtraTreesRegressor' is trained on only the output of receiver #1, an RMSE of $3.30 \pm 0.33$ and $R^2$ of 0.94 is achieved, and using receiver #2, an RMSE of $3.40 \pm 0.37$ and $R^2$ of 0.94 is achieved. This highlights the ability of this method to operate effectively with a limited number of sensors, and suggests that the benefit of introducing more receivers will not be seen until more hotspots are introduced.

## 4. Conclusions

This work investigated the application of ultrasonic guided waves for temperature monitoring of printed circuit board (PCB) components. Specifically, three different PCB configurations were tested to assess the effectiveness of our novel approach. By leveraging machine learning models, we have successfully demonstrated the temperature prediction of known hotspot locations on the PCBs. This was achieved simultaneously for five different components using only two or three UGW sensors, showcasing the efficiency of this method.

Ensemble-based regression models, including techniques like Random Forests and Gradient Boosting, were found to outperform traditional linear regression models, as well as neural networks, in predicting temperature with high accuracy. The most accurate predictions were achieved by selecting the top 10+ features that exhibited the highest correlation with the target variable, as determined by the mutual information regression score. This feature selection process helped the models capture the key relationships between the sensor data and temperature, leading to more precise results.

By operating this method at a high sampling rate, temperature fluctuations could be tracked over time, providing early detection of potential hotspots on the PCB. This ability is crucial for preventing damage or failure in sensitive electronic components, where excessive heat build-up can degrade performance or lead to irreversible damage. Early identification of these hotspots would allow for preventive measures to be taken, ensuring better reliability and safety in electronic systems.

In cases where the potential hotspot positions are unknown, or if higher spatial resolution is needed, we propose a novel method of automating the process of training machine learning models. A rig could be constructed with a mechanical two-axis control

mechanism, such as a CNC plotter equipped with stepper motors and rails. This system would allow precise control over the positioning of a soldering iron or other heat-generating devices to apply heat at evenly spaced points across the PCB. This automated approach would enable the collection of a large dataset for training purposes, allowing the models to generalize better across different hotspot locations.

While the results of this study are promising, there are several limitations that should be acknowledged. Firstly, the study focused on a limited number of PCB configurations and hotspot positions, and additional testing is required to fully evaluate how effective the proposed method is across different PCB designs and operational conditions. At present, the size of a board that this method is applicable to is a limiting factor, as placing PWAS on very small PCBs could cause short circuit faults across traces. If necessary, a PCB could be designed with this type of temperature measurement in mind, integrating the sensors into the circuit, in order to eliminate this issue. This would also reduce the chances of damage caused to the board during the soldering of external PWAS.

Secondly, the machine learning models were trained on relatively small, constrained datasets, and their performance may vary under different conditions. Additionally, The use of external heating to simulate component temperatures, while effective, may not perfectly mimic the thermal dynamics of actual operating conditions. Finally, the spatial resolution of the system has not been fully investigated, and further research is needed to optimize sensor configurations for different PCB designs.

Moving forward, we aim to explore the spatial resolution limitations of the UGW-based temperature monitoring system. Understanding the minimum distance between two hotspots that can be accurately detected is vital for refining the system's performance. We will also investigate the optimal configuration for sensor placement, including the ideal number, size, and positioning of the UGW sensors to maximize accuracy and coverage.

Another area that we are interested in exploring is the use of digital twins. By creating a digital replica of the PCB system, models could be trained on simulated data before being deployed in real-world scenarios. This approach would expedite the model training process, reducing the need for extensive experimental setups while still ensuring robust model performance. The use of digital twins could also allow for virtual testing of various PCB configurations, sensor placements, and environmental conditions, leading to more efficient and cost-effective development of the temperature monitoring system.

With our approach, we have demonstrated an improvement over traditional methods in terms of cost-effectiveness and real-time monitoring capabilities. Unlike thermocouples, which require direct contact and are impractical for comprehensive coverage, our method uses a minimal number of sensors to achieve accurate temperature predictions across multiple hotspots. Compared to thermal cameras, which can be expensive and less effective for real-time monitoring, our approach offers a more affordable and scalable solution. Additionally, while onboard chip temperature sensors are effective for specific ICs, they do not provide a holistic view of the PCB's thermal state. Our method addresses this gap by leveraging machine learning to interpret complex ultrasonic guided wave signals, providing a comprehensive and real-time temperature monitoring solution for PCBs.

In conclusion, ultrasonic guided waves, in conjunction with machine learning, offer a promising solution for real-time temperature monitoring of PCB components. The method's scalability, accuracy, and potential for early hotspot detection make it a valuable tool for enhancing the safety and reliability of electronic systems. With further advancements in sensor technology, automated training processes, and digital twin simulations, this technique could become a standard approach in thermal management for complex, safety-critical electronic systems.

**Author Contributions:** Conceptualization, methodology, software development, validation, data collection, analysis, writing: L.Y. Conceptualization, supervision, draft preparation, review, and editing: N.H., M.H., and B.Z. All authors have read and agreed to the published version of the manuscript.

**Funding:** This work was supported by the University of Southampton, and EPSRC grant EP/T517859/1.

**Data Availability Statement:** The data presented in this study are openly available on GitHub at https://github.com/Lrrrence/PCB-temp-monitoring (accessed on 23 December 2024).

**Conflicts of Interest:** The authors declare no conflicts of interest.

## References

1. Ling, Q.; Isa, N.A.M. Printed Circuit Board Defect Detection Methods Based on Image Processing, Machine Learning and Deep Learning: A Survey. *IEEE Access* **2023** , *11*, 15921–15944. [CrossRef]
2. Kaya, G.U. A Novel Hybrid Optical Imaging Sensor for Early Stage Short-Circuit Fault Diagnosis in Printed Circuit Boards. *Trait. Signal* **2024**, *41*, 531–542. [CrossRef]
3. Ustabas Kaya, G. Development of hybrid optical sensor based on deep learning to detect and classify the micro-size defects in printed circuit board. *Measurement* **2023**, *206*, 112247. [CrossRef]
4. Shaukatullah, H.; Claassen, A. Effect of thermocouple wire size and attachment method on measurement of thermal characteristics of electronic packages. In Proceedings of the Ninteenth Annual IEEE Semiconductor Thermal Measurement and Management Symposium, San Jose, CA, USA, 11–13 March 2003. [CrossRef]
5. Janeczek, K.; Araźna, A.; Stęplewski, W.; Kościelski, M.; Lipiec, K.; Rafalik, I.; Karolewski, S.; Liszewska, D.; Sitek, A. Investigations of temperature sensor embedded into PCB. *MicroElectron. Int.* **2020**, *37*, 199–204. [CrossRef]
6. Sarawade, A.; Charniya, N. Detection of Faulty Integrated Circuits in PCB With Thermal Image Processing. In Proceedings of the 2019 International Conference on Nascent Technologies in Engineering (ICNTE 2019), Navi Mumbai, India, 4–5 January 2019.
7. Dong, Z.; Chen, L. Image registration in PCB Fault Detection Based on Infrared Thermal Imaging. In Proceedings of the 2019 Chinese Control Conference (CCC). Technical Committee on Control Theory, Chinese Association of Automation, Guangzhou, China, 27–30 July 2019. [CrossRef]
8. Baker, N.; Lemmon, A.; Iannuzzo, F.; Bęczkowski, S.; Austin, J.; Ostrander, L. Temperature Monitoring of Multi-Chip SiC MOSFET Modules: On-Chip RTDs vs. VSD(T). In Proceedings of the 2023 25th European Conference on Power Electronics and Applications (EPE'23 ECCE Europe), Aalborg, Denmark, 4–8 September 2023; pp. 1–9. [CrossRef]
9. Kasemsadeh, B.; Heng, A.; Ashara, A. Temperature Sensors: PCB Guidelines for Surface Mount Devices. Application Report SNOA967A. Texas Instruments. Available online: https://www.ti.com/lit/an/snoa967a/snoa967a.pdf (accessed on 19 October 2024).
10. Lam, T.L. Low-Cost Non-Contact PCBs Temperature Monitoring and Control in a Hot Air Reflow Process Based on Multiple Thermocouples Data Fusion. *IEEE Access* **2020**, *9*, 123566–123574. [CrossRef]
11. Leite, T.M.; Freitas, C.; Magalhães, R.; Silva, A.F.; Alves, J.R.; Viana, J.C.; Delgado, I. Temperature Calibration for Distributed Temperature Sensing of Printed Circuit Boards using Optical Fiber Sensors. *IEEE Trans. Components Packag. Manuf. Technol.* **2023**, *13*, 1380–1387. [CrossRef]
12. Yan, D.; Yang, Y.; Hong, Y.; Liang, T.; Yao, Z.; Chen, X.; Xiong, J. Low-Cost Wireless Temperature Measurement: Design, Manufacture, and Testing of a PCB-Based Wireless Passive Temperature Sensor. *Sensors* **2018**, *18*, 532. [CrossRef]
13. Arun Ramakrishnan, M.G.P. A life consumption monitoring methodology for electronic systems. *IEEE Trans. Components Packag. Technol.* **2003**, *26*, 625–634. [CrossRef]
14. Mitra, M.; Gopalakrishnan, S. Guided wave based structural health monitoring: A review. *Smart Mater. Struct.* **2016**, *25*, 053001. [CrossRef]
15. Kang, S.H.; Kang, M.; Kang, L.H. Defect detection on the curved surface of a wind turbine blade using piezoelectric flexible line sensors. *Struct. Health Monit.* **2022**, *21*, 1207–1217. [CrossRef]
16. Shang, L.; Zhang, Z.; Tang, F.; Cao, Q.; Pan, H.; Lin, Z. CNN-LSTM Hybrid Model to Promote Signal Processing of Ultrasonic Guided Lamb Waves for Damage Detection in Metallic Pipelines. *Sensors* **2023**, *23*, 7059. [CrossRef] [PubMed]
17. Wang, Y.; Qiu, L.; Luo, Y.; Ding, R. A stretchable and large-scale guided wave sensor network for aircraft smart skin of structural health monitoring. *Struct. Health Monit.* **2019**, *20*, 861–876. [CrossRef]
18. Ge, H.; Huat, D.C.K.; Koh, C.G.; Dai, G.; Yu, Y. Guided wave–based rail flaw detection technologies: State-of-the-art review. *Struct. Health Monit.* **2022**, *21*, 1287–1308. [CrossRef]
19. Jia, Y.; Skliar, M. Ultrasonic Measurements of Temperature Distribution and Heat Fluxes Across Containments of Extreme Environments. In Proceedings of the 2019 IEEE International Ultrasonics Symposium (IUS), Glasgow, UK, 6–9 October 2019. [CrossRef]

20. Zhang, Y.; Cegla, F. Co-located dual-wave ultrasonics for component thickness and temperature distribution monitoring. *Struct. Health Monit.* **2022**, *22*, 1090–1104. [CrossRef]
21. Liu, H.; Zhou, Z.; Lou, L. Wireless Temperature Measurement for Curved Surfaces Based on AlN Surface Acoustic Wave Resonators. *Micromachines* **2024**, *15*, 562. [CrossRef] [PubMed]
22. Lee, Y.J.; Khuri-Yakub, B.; Saraswat, K. Temperature measurement in rapid thermal processing using the acoustic temperature sensor. *IEEE Trans. Semicond. Manuf.* **1996**, *9*, 115–121. [CrossRef]
23. Klimek, D.; Anthonyt, B.; Abbate, A.; Kotidis, P. Laser Ultrasonic Instrumentation for Accurate Temperature Measurement of Silicon Wafers in Rapid Thermal Processing Systems. *MRS Online Proc. Libr. (OPL)* **1998**, *525*, 135. [CrossRef]
24. Yule, L.; Harris, N.; Hill, M.; Zaghari, B.; Grundy, J. Temperature Hotspot Detection on Printed Circuit Boards (PCBs) Using Ultrasonic Guided Waves—A Machine Learning Approach. *Sensors* **2024**, *24*, 1081. [CrossRef]
25. Pedregosa, F.; Varoquaux, G.; Gramfort, A.; Michel, V.; Thirion, B.; Grisel, O.; Blondel, M.; Prettenhofer, P.; Weiss, R.; Dubourg, V.; et al. Scikit-learn: Machine Learning in Python. *J. Mach. Learn. Res.* **2011**, *12*, 2825–2830.
26. Yu, L.; Santoni-Bottai, G.; Xu, B.; Liu, W.; Giurgiutiu, V. Piezoelectric wafer active sensors for in situ ultrasonic-guided wave SHM. *Fatigue Fract. Eng. Mater. Struct.* **2008**, *31*, 611–628. [CrossRef]